Proceedings of Machine Learning Research vol 145:223–252, 2021 2nd Annual Conference on Mathematical and Scientific Machine Learning

Numerical Calabi-Yau metrics from holomorphic networks

Michael R. Douglas* MDOUGLAS@SCGP.STONYBROOK.EDU
Subramanian Lakshminarasimhan† SUBRAMANIAN.LAKSHMINARASIMHAN@STONYBROOK.EDU
Yidi Qi YIDI.QI@STONYBROOK.EDU
Department of Physics, YITP and SCGP, Stony Brook University
† *Department of Applied Mathematics and Statistics, Stony Brook University*
∗ *Center of Mathematical Sciences and Applications, Harvard University*

Editors: Joan Bruna, Jan S Hesthaven, Lenka Zdeborova

Abstract

We propose machine learning inspired methods for computing numerical Calabi-Yau (Ricci flat Kähler) metrics, and implement them using Tensorflow/Keras. We compare them with previous work, and find that they are far more accurate for manifolds with little or no symmetry. We also discuss issues such as overparameterization and choice of optimization methods.

Keywords: Calabi-Yau metrics, high dimensional PDEs, feedforward networks, complex geometry

1. Introduction

Kähler manifolds with Ricci flat metrics, known as Calabi-Yau manifolds, are the first and still the most important starting point for compactification of string theory to produce realistic physical models. Their study led to the discovery of mirror symmetry and a great deal of interesting mathematics. A brief survey appears in Douglas (2015), and textbooks on mirror symmetry include Hori et al. (2003); Aspinwall et al. (2009).

No closed form expressions are known for these Ricci flat metrics, and it is generally believed that none exist.[1] One can get an approximate description using methods of numerical general relativity, as pioneered in Headrick and Wiseman (2005). The special properties of Kähler geometry lead to many simplifications, starting with the representation of the metric by a single function. Donaldson introduced many ideas such as a representation by projective embeddings and approximation by balanced metrics (Donaldson, 2009). Subsequent works simplified and improved the numerical methods (Douglas et al., 2007, 2008; Doran et al., 2008; Bunch and Donaldson, 2008; Seyyedali, 2009; Braun et al., 2008a,b; Headrick and Nassar, 2013; Anderson et al., 2010a,b, 2012) so that a fairly simple program can get accurate results.

To simplify a bit, the approach used in these works is to expand the Kähler potential in a polynomial basis. As is the case for spectral methods, this is very good for approximating smooth functions with variations on length scales $1/k$, where k is the order of the polynomials used. This is sometimes good enough, but by varying moduli one can easily produce metrics with structure on arbitrarily short scales, say by approaching a singular limit, as was studied in Cui and Gray (2020). And since on a D-dimensional manifold, the number of basis functions grows as $\mathcal{O}(k^D)$, one cannot take k very large (the "curse of dimensionality"). Indeed, almost all of these works restrict attention

1. But see Gaiotto et al. (2010); Kachru et al. (2020) for an analytic approach to the K3 metric.

to manifolds with large discrete symmetry groups to get a manageable number of coefficients. An exception is Braun et al. (2008a) which studied a randomly chosen quintic with no symmetry.

In recent years, there has been much success with machine learning (ML) inspired approaches to scientific computation, and especially the solution of PDE's such as Navier-Stokes and the Schrödinger equation. This is a rapidly developing area and any reviews we cite here would become dated very quickly, but to give a simple illustration of the approach we follow we cite Hoyer et al. (2019). This work solves problems in structural optimization – mathematically, the unknown is a single function in a bounded domain of $\mathbb{R}^2$ and the solution is the minimum of a nonlocal energy functional (the integrated stress). What is novel is to represent the unknown function, not in terms of finite elements or a Fourier basis, but as the output of a neural network. This provides a space of approximating functions parameterized by the network weights, which can be efficiently computed using technologies developed for machine learning. Standard numerical optimization applied to the energy considered as a function of the weights leads to high quality solutions, which are not limited by the constraints of previous methods.

These methods have only begun to be explored for higher dimensional geometry. The idea we propose and study here is to represent the Kähler potential in terms of the output of a **holomorphic network** or a **bihomogeneous network**. Both are feedforward neural networks, whose inputs are simple functions of the complex coordinates, which use the activation function $z \to z^2$, and whose outputs are efficiently computable functions of the weights. We then find the metric in this class which is closest to Ricci flat by numerical optimization of an error function with respect to the weights, much as was done for highly symmetric metrics in Headrick and Nassar (2013).

For the holomorphic network, the inputs are complex coordinates or low degree sections, the weights and intermediate values (or "activations") are complex, and the outputs are a subspace of the space of holomorphic sections. One then takes a hermitian combination of these outputs and their complex conjugates to get a Kähler potential.

By contrast, in the bihomogeneous network, the inputs are the real and imaginary parts of products of holomorphic and antiholomorphic functions, homogeneous in each separately. Thus the weights and intermediate values can be taken to be real. The output of the network is then used as a Kähler potential. This turns out to work better than the holomorphic network for reasons we will explain.

Since each layer doubles the degree of the section, in principle one can work with large values of k. One faces the standard challenges of deep networks such as exploding gradients, but we were able to use depths up to 5 without this being a problem.

Our formulation of the numerical Calabi-Yau metric problem is formally very similar to supervised learning – both problems amount to fitting a function given a set of input-output values (x_i, y_i), where x_i is sampled from an input distribution and y_i is known. Thus most of the task is already implemented in standard ML packages, and one only needs a few domain dependent additions. Our code uses TensorFlow, and is available on Github.[2]

We obtain results for a variety of quintic hypersurfaces, including the familiar one-parameter Dwork family, and also hypersurfaces with little or no symmetry. Our main focus is to understand the accuracy of these metrics and its dependence on parameters, both those of the manifold and hyperparameters (parameters of the model and learning algorithm). We can get mean errors (MAPE defined below) around 10^{-3} for metrics with no symmetry, about 100 times better than

2. https://github.com/yidiq7/MLGeometry

Braun et al. (2008a). We also discuss the nature of the optimization landscape and the overparameterized regime, which have been important themes in recent studies of ML.

1.1. Related work

Recent works which study numerical Calabi-Yau geometry include Ashmore et al. (2020); Ashmore (2020); Anderson et al. (2020). In Ashmore et al. (2020), the Kähler potential is represented by a gradient boosted decision tree. The problem is solved at various lower degrees k, and the ML model does extrapolation in the degree (Richardson extrapolation). In Ashmore (2020) eigenvalues of Hodge Laplacians are computed. The work Anderson et al. (2020) (appearing simultaneously with ours) studies metrics with $SU(3)$ structure using neural networks.

Polynomial activation functions have been studied in many ML works, for example Chrysos et al. (2020); Mannelli et al. (2020), but our motivations (contact with higher dimensional complex geometry) are new.

A brief mathematical summary of the approach will appear in Douglas (2020).

2. Numerical complex geometry using machine learning methods

In this section we alternate between the complex geometry needed for our problem and review of the concepts we use from machine learning. For the benefit of readers who are not experts in both fields, we review some basic concepts on both sides in Appendix B. Some useful background material includes Griffiths and Harris (2014); Huybrechts (2005) on complex geometry and Bishop (2013) on machine learning.

2.1. Brief review of the Calabi-Yau metric problem

Our problem is the following: we are given a complex manifold M with local coordinates $z^i \equiv (z^1, \ldots, z^n)$ and their complex conjugates $\bar{z}^{\bar{i}} \equiv (z^1, \ldots, z^n)^*$. which admits Kähler metrics, determined (as we review in Appendix B.1) by a Kähler potential K as

$$g_{i\bar{j}} = \frac{\partial^2 K}{\partial z^i \partial \bar{z}^{\bar{j}}} \equiv \partial_i \bar{\partial}_{\bar{j}} K. \tag{1}$$

We want to find a Kähler metric which to a good approximation satisfies Einstein's equation

$$\text{Ricci}_{i\bar{j}} = \Lambda \, g_{i\bar{j}}, \tag{2}$$

where Λ is a real constant. General arguments determine the sign of Λ in terms of the topology of M (its first Chern class). Deep mathematical theorems of Yau, Aubin, Donaldson-Song, and others, show that a solution always exists for $\Lambda \leq 0$, and give the necessary and sufficient conditions for $\Lambda > 0$. For $\Lambda \neq 0$ the solution is generally unique, while for $\Lambda = 0$ it is unique up to an overall rescaling $g_{i\bar{j}} \to R^2 g_{i\bar{j}}$ for $R \in \mathbb{R}^+$. The $\Lambda = 0$ metrics are called "Ricci flat." While we focus on this case, the methods we discuss can be used for the other cases.

In this work we take M to be the quintic hypersurface in $\mathbb{CP}^4$, the set of solutions to a polynomial equation such as

$$0 = f(Z^1, Z^2, Z^3, Z^4, Z^5) = \sum_{i=1}^{5} (Z^i)^5 + \psi Z^1 Z^2 Z^3 Z^4 Z^5 \tag{3}$$

where ψ is a fixed complex number (a "complex modulus"). Here Z^i are projective coordinates, and a point on $\mathbb{CP}^4$ is an equivalence class of points in $\mathbb{C}^5 - \{\mathbf{0}\}$ under $Z^i \sim \lambda Z^i \, \forall \, \lambda \in \mathbb{C}$. M is a three complex dimensional space which is a manifold, except at possible singular points Z at which

$$0 = f(Z) = \partial_i f(Z) \; \forall 1 \leq i \leq 5. \tag{4}$$

For Equation (3), these only exist for $\psi = -5\omega$ where $\omega^5 = 1$ is a fifth root of unity. For other ψ, one can show that $c_1(M) = 0$, so $\Lambda = 0$ in Equation (2). This Fermat quintic (for $\psi = 0$) or Dwork family of quintics is the most studied example, *e.g.* see Candelas et al. (1991).

More generally, one can take f to be any quintic polynomial. Such a polynomial has 126 adjustable coefficients, and two manifolds M_1 and M_2 defined in terms of two polynomials f_1, f_2 are equivalent (complex diffeomorphic) only if there exists a linear transformation $W^i \equiv L^i_j Z^j$ such that $f_1(Z) = f_2(W)$. This introduces 25 redundancies in the parameterization, so the space parameterizing quintic hypersurfaces in $\mathbb{CP}^4$ (the complex moduli space) is 101 complex dimensional. One can show that solutions of Equation (4) only exist on a codimension one variety in this space (the "discriminant locus" Δ), so the moduli space of nonsingular quintic CY manifolds is 101 dimensional.

Of the many generalizations of this construction, the most used in string theory are to replace $\mathbb{CP}^N$ by products of projective spaces, weighted projective spaces and toric varieties. Here we simply point out that the constructions below can be straightforwardly adapted, by replacing homogeneity with weighted multihomogeneity, or equivalently gauge invariance in the GLSM constructions. Many details of these generalizations can be found in the works of the Penn group (Braun et al., 2008b; Anderson et al., 2010a).

2.2. The embedding method and geometric quantities

Following Donaldson (2009), most work on numerical Calabi-Yau metrics represents the metric using an embedding by holomorphic sections of a very ample line bundle $\mathcal{L}$. This embedding is a map into a linear space, analogous to spectral embeddings such as the "Laplacian eigenmap" construction, but with the great advantage that the map has a simple exact form. A review of the embedding method is in Appendix B.2.

The embedding representation gives us a natural family of metrics, the pullbacks of the Fubini-Study metrics from complex projective space. Using our embedding by a basis of N sections s^I, and pulling back a Fubini-Study metric on $\mathbb{CP}^{N-1}$, the embedding then leads to the Kähler potential

$$K = \log \sum_{I,\bar{J}} h_{I,\bar{J}} s^I \bar{s}^{\bar{j}} \tag{5}$$

where s^I is a basis of $N = h_0(\mathcal{L})$ holomorphic sections. This gives us an N^2 real dimensional family of metrics parameterized by the hermitian matrix $h_{I,\bar{J}}$.

The geometry of a Calabi-Yau manifold (let n be its complex dimension; eventually we will take $n = 3$) is determined by two fundamental differential forms. The first is present on any Kähler manifold – it is the Kähler form

$$\omega = \partial_i \partial_{\bar{j}} K \, dZ^i \wedge d\bar{Z}^{\bar{j}}. \tag{6}$$

This carries the same information as the metric and can be used to write the volume element $d\mu_g = \sqrt{g}$. On a Kähler manifold, one can do this without taking square roots:

$$d\mu_g \equiv \omega_g^{\dim_{\mathbb{C}} M} = \det \omega_g = \det_{i,\bar{j}} \partial_i \partial_{\bar{j}} K. \tag{7}$$

The other, which is only present for a Calabi-Yau manifold, is the holomorphic n-form

$$\Omega = \Omega_{i_1 \dots i_n} dZ^1 \wedge \dots \wedge dZ^n. \tag{8}$$

It is nonvanishing and nonsingular, so we can define an associated volume form

$$d\mu_\Omega \equiv \mathcal{N}_\Omega \Omega \wedge \bar{\Omega}. \tag{9}$$

The normalization constant $\mathcal{N}_\Omega$ will be set to make the total integrals of both volume forms equal. One can show that the integral $\int_M \omega_g^n$ is a topological invariant, which stays fixed as we continuously vary the metric. Thus we can begin by computing the value of $\mathcal{N}_\Omega$ which does this for the initial metric, and leave it fixed as we search for the Ricci flat metric.

The form Equation (9) depends on the complex structure but is independent of the Kähler form and thus the embedding we use to represent M. Often one can write an explicit formula for it – for a hypersurface it is

$$\Omega = \frac{dZ^1 \wedge \dots \wedge dZ^n}{\partial f / \partial Z^{n+1}} \tag{10}$$

where f is as in Equation (3). This formula becomes singular where $\partial f / \partial Z^{n+1} = 0$. To fix this, one can check that one gets the same Ω by choosing any of other the coordinates to play the role of Z^{n+1}. One can then define several coordinate patches, each with one of these representatives, and whose union covers M.

Now, we come to a very helpful simplification which follows from Calabi-Yau geometry. For a general metric, Equation (2) is a system of PDEs determining the individual metric components and with general covariance. It is not elliptic unless one properly fixes the coordinate system, which is quite nontrivial to do. By using complex coordinates, Equation (1) for the metric, and Equation (38) for the Ricci tensor, it becomes a PDE for a single function without these issues.

$$0 = \frac{\partial^2}{\partial Z^i \bar{\partial} \bar{Z}^{\bar{j}}} \log \det_{i,\bar{j}} \frac{\partial^2 K}{\partial Z^i \bar{\partial} \bar{Z}^j}. \tag{11}$$

However this is still nonlinear and involves many derivatives. But for a Ricci flat Kähler metric, one can integrate this formula twice to obtain

$$d\mu_\Omega = d\mu_g \tag{12}$$

or equivalently

$$1 = \eta \equiv \frac{d\mu_g}{d\mu_\Omega} \tag{13}$$

where the constants of integration are determined by global consistency.[3] Another advantage of this condition is that it can be obtained from a convex energy functional (see §3).

To make this completely explicit, use Equation (10), use the constraint $f = 0$ to solve for $i, j = n+1$ in the determinant in terms of the other derivatives, and make a final rearrangement, to get

$$1 = \eta \equiv \frac{1}{\mathcal{N}_\Omega} |\partial f / \partial Z^{n+1}|^2 \det_{1 \le i,j \le n} L_i^{i'} \frac{\partial^2 K}{\partial Z^{i'} \bar{\partial} \bar{Z}^{j'}} (L^\dagger)_j^{j'}, \tag{14}$$

where the matrix L is given explicitly in Equation (40).

3. A short argument for this is that if it were not the case, then $1/\eta$ in Equation (14) would define a non-constant harmonic function on M, but on a compact M this does not exist.

2.3. Multilayer holomorphic embeddings

The idea we will pursue in this work is to use the feed-forward network:

$$F_w = W^{(d)} \circ \theta \circ W^{(d-1)} \circ \ldots \circ \theta \circ W^{(1)} \circ \theta \circ W^{(0)}, \tag{15}$$

where the $W^{(i)}$'s are general linear transformations, and θ is the activation function, to define a subset of the metrics Equation (5). There are several ways to do this. In this subsection we define a network with complex weights and activations, which defines a subspace of $H^0(\mathcal{L}^k)$. We will then restrict Equation (5) to this subspace. In the next subsection we will take a different approach, forming real combinations as the inputs to the network.

Thus, here we take the input space $\mathcal{X}$ to be the ambient space $H^0(\mathcal{O}_M(1))$, the space parameterized by the homogeneous coordinates Z^i. Concretely, the first layer has 5 complex inputs. We take all of the intermediate vectors to be complex, and we choose $\theta(x)$ to be a nonlinear homogeneous holomorphic function. The simplest choice and the one we will use is to take

$$\theta(x) = x^2. \tag{16}$$

Thus each successive layer defines a subspace of sections of degree twice the previous layer.

To get a real valued Kähler potential, we replace the final layer $W^{(d)}$ with a general linear combination of products of the sections with their complex conjugates,

$$\begin{aligned} K(w;Z) &= \log \sum_{i_d=1,\bar{j}_d=1}^{D_d} h^{(d)}_{i_d,\bar{j}_d} Z_d^{i_d} \bar{Z}_d^{\bar{j}_d} && (17)\\ Z^{(d)} &\equiv \theta \circ W^{(d-1)} \circ \theta \circ \ldots \circ \theta \circ W^{(1)} \circ \theta \circ W^{(0)} Z && (18)\\ \bar{Z}^{(d)} &\equiv (Z^{(d)})^*. && (19) \end{aligned}$$

This construction gives us a class of metrics for each choice of depth d and layer widths $D_1, \ldots, D_d$, obtained from embeddings with degree $k = 2^d$. The total number of real weights is

$$N_w = 2\left(DD_1 + D_1D_2 + \ldots + D_{d-1}D_d\right) + D_d^2. \tag{20}$$

Generally $D_i < h_0(\mathcal{L}^{2^i})$ so this will not span the complete basis of sections, in other words we have restricted the embedding and are only using a subset of metrics. While the final layer z_d is a linear subspace of $H^0(\mathcal{L}^{2^d})$, this subspace is nonlinearly parameterized by the weights. The hope is that it is flexible enough to describe the metrics of interest.

A variation on this is to take the inputs Z to be a complete basis of sections s^I of degree k_0. For the hypersurface $f = 0$ in $\mathbb{CP}^{D-1}$, the basis will be the symmetrized degree k_0 monomials, quotiented by the ideal generated by f (if $k_0 \geq \deg f$). Other combinations of layers and activation functions are of course possible, subject to the constraint that every activation (intermediate value) is homogeneous (a section of a definite line bundle). Thus one cannot have skip connections, but one could take other products of outputs from previous layers.

We have implemented these networks, but they turned out to have some disadvantages compared to the approach we will discuss next. One is technical: ML software does not always treat holomorphic functions as one would expect (in particular the derivative $\partial/\partial z$), and one must be

careful in programming a complex network. More importantly, one needs very wide networks to represent simple metrics. Consider the Kähler potential

$$K = \log \sum_i |Z^i|^2 \tag{21}$$

constructed from $k = 1$ sections. This is also a point in every space of $k > 1$ metrics (up to the overall scale), as we can write

$$\begin{aligned} K &= k \log \sum_i |Z^i|^2 = \log \left(\sum_i |Z^i|^2 \right)^k && (22) \\ &= \log \sum_I c_I |Z^{I_1} \cdot \ldots \cdot Z^{I_k}|^2. && (23) \end{aligned}$$

Reproducing this sum over the complete basis of sections would require a very wide final layer.

2.4. Bihomogeneous embeddings

A variation which does not have the problems we just described is to use bihomogeneous sections, meaning products of holomorphic and antiholomorphic sections, as the activations (intermediate values) of the network. Thus, we would take

$$K(w; Z) = \log W^{(d)} \circ \theta \circ W^{(d-1)} \circ \ldots \circ \theta \circ W^{(2)} \circ \theta \circ W^{(1)}(Z\bar{Z}), \tag{24}$$

where the inputs $(Z\bar{Z})$ are the real and imaginary parts of the bihomogeneous (or "sesquilinear") combinations $Z^I \bar{Z}^{\bar{J}}$. In terms of $Z^I = X^I + iY^I$ these are

$$\begin{aligned} & X^I X^J + X^J X^I - Y^I Y^J - Y^J Y^I \qquad \forall 1 \leq I \leq J \leq n, && (25) \\ & X^I Y^J - X^J Y^I \qquad \forall 1 \leq I < J \leq n, && (26) \end{aligned}$$

which in n complex dimensions make up n^2 real components. The output dimension is $D_d = 1$. For $d = 1$ and taking $W^{(1)}$ real, this reproduces Equation (5) with $k = 1$.

In this network, the inputs, intermediate variables and all of the weight matrices will be real. One still needs the activation function θ to be homogeneous, and $z \to z^2$ is still the natural choice. The total number of real weights is now

$$N_w = DD_1 + D_1 D_2 + \ldots + D_{d-2} D_{d-1} + D_{d-1}. \tag{27}$$

Let us check that this transforms properly under a change of projective coordinates $z^i \to \lambda z^i$. Then

$$\begin{aligned} (Z\bar{Z}) &\to |\lambda|^2 (Z\bar{Z}) && (28) \\ \theta \circ W(Z\bar{Z}) &\to |\lambda|^4 \theta \circ W(Z\bar{Z}) && (29) \\ &\vdots && (30) \\ K(w; Z) &\to K(w; Z) + 2^{d-1} \log |\lambda|^2 && (31) \end{aligned}$$

Again, there are many variations on this construction – any rules of combination which are homogeneous in the bidegrees $(1, 0)$ for z and $(0, 1)$ for $\bar{z}$ are allowed.

With this construction, the higher degree space of Kähler potentials contains the lower degree spaces in a simple way. For example, Equation (22) can be reproduced with width 1 intermediate layers. This construction can also represent real-valued functions as a difference $K_1 - K_2$. Here K_2 could be a fixed reference Kähler potential of the same degree, or the output of a second network.

A potential problem with Equation (24) is that it is not easy to enforce positive definiteness of Equation (1). However we got good results without explicitly doing so. Two reasons are that we do not use the inverse metric, and Equation (12) forces the determinant of the metric to be positive.

3. Implementation

Other than the use of a network instead of a basis of sections, our method is as used in previous works: optimization as in Headrick and Nassar (2013) using the sampling methods of Douglas et al. (2008). It turns out that this is so similar to supervised learning that we can easily adapt standard ML software to do it.[4] Thus we review supervised learning briefly (and at more length in appendix B.4) to explain this.

3.1. General implementation

In supervised learning, we have a data set of N_{data} items, each of which is an input-output pair (x_n, y_n). These are supposed to be drawn from a probability distribution $\mathcal{P}$ on $\mathcal{X} \times \mathcal{Y}$. The goal is to choose the function from $\mathcal{X}$ to $\mathcal{Y}$ from a given set (or "model") which best describes the general relation $\mathcal{P}$ between input and output, in the sense that it minimizes some definition of the expected error (an objective or "loss" function). The procedure of making this choice given the data set is called training the network.

To phrase our problem in these terms, note that in Equation (12), the left hand side $d\mu_\Omega$ is a known function of the point Z, while the right hand side $d\mu_g$ is an adjustable function depending on the parameters of the metric g, in other words the weights. Thus we can take our input dataset x_i to be a set of points Z_i, the output we are trying to fit is the value of $d\mu_\Omega$ at these points, call these y_i, and the "model" we are using to fit it is $d\mu_g$. Thus the problem is exactly of the form we desired. We are still solving a PDE, but the derivatives are all done in the computation of $d\mu_g$.

Let us flesh out this observation. An interpolation problem requires a sampling procedure for the x_i, a model for the y_i, an objective function which measures the quality of the fit, and an optimization procedure.

As we just explained, the Ricci flatness condition is $\eta = 1$. The least squares error is then

$$\mathcal{E} = \int_M d\mu_{ref} \, (\eta - 1)^2 \tag{32}$$

where $d\mu_{ref}$ is a "reference measure" on M. Here η (Equation (12)) is implicitly a function of the weights through $d\mu_g$; we put this in the numerator to simplify this dependence. Varying with respect to the weights, and assuming that there are enough weights to vary η at every point in the support of $d\mu_{ref}$, its minimum will be $\eta = 1$ on this support.

Note that the integral of any convex function $F(\eta)$ will have the same optimum. Out of these choices, we would prefer to use an objective function which is convex in the parameters. An important feature of the continuum PDE is that if $F(\eta)$ is convex, then considered as a functional of

4. Supervised learning was already used in computing numerical Ricci flat metrics by Ashmore et al. (2020), to extrapolate the results from Donaldson's T-map method. We feel the approach taken here is more straightforward.

the Kähler potential, $\mathcal{E}_F$ has a unique critical point.[5] However this need not be so when considered as a function of the parameters. Indeed, it is never the case for a nontrivial objective function and the multilayer FFN Equation (15), as is clear for the simplest example of a two layer linear network $y = w_1 w_0 x$.

Another complicating factor is that we will use a reference measure $d\mu_{ref}$ supported on a finite set of points. Since the variation of $\mathcal{E}_F$ only imposes constraints on the support of $d\mu_{ref}$, the variational equations and their solutions will generally depend on this support (but not on the values of $d\mu_{ref}$). Furthermore one expects multiple or degenerate solutions in the overparameterized regime we discuss later.

In practical ML, while nonconvexity and nonuniqueness can lead to problems, they turn out not to be as serious as one might expect. This point has received extensive study and can be understood analytically for linear networks (with activation function $f(x) = x$), see for example Advani et al. (2020). But in practice, one varies the initial conditions and learning rate until one finds choices which work, as discussed in textbooks such as Goodfellow et al. (2016). This is part of the "art" of machine learning.

As for the objective function, least squares as in Equation (32) is usually a good choice, though we consider alternatives in §4.1. As a reference measure, we take the Monte Carlo measure (or "empirical measure") defined as an average over a set of N randomly chosen points on M,

$$d\mu_{ref}(x) = \frac{1}{N}\sum_{i=1}^{N} \delta(x - x_i). \tag{33}$$

If x_i is sampled from some dP, then $\lim_{N\to\infty} d\mu_{ref} \to dP$ under very weak conditions on dP and the integrand.

To sample points on M we use the procedure of Douglas et al. (2008). We sample pairs of points a, b from a normal distribution on $\mathbb{C}^5$. Regarded as points on $\mathbb{CP}^4$, they are distributed according to Equation (39). We then find the points on the intersection of the line $\lambda a + \rho b$ with M, in other words the choices of λ/ρ for which $f(\lambda a + \rho b) = 0$. This equation will have $\deg f$ solutions (with multiplicity) and for our purposes (which do not look at correlations between points) we can use all of them as inputs x_n. By a theorem of Shiffman and Zelditch (1999), they are distributed according to the pullback of Equation (39) to M. We then reweighted this distribution to get $d\mu_{ref} = d\mu_\Omega$, by multiplying by the ratio of this form over the FS volume form. In this way we avoided introducing an additional geometric quantity not present in the actual CY geometry. This was important for the balanced metric computation of Douglas et al. (2008), but for defining a loss function it is not strictly necessary.

3.2. Implementation details

Our code is written in Python 3 and uses TensorFlow, numpy and sympy. Many of the routines are written twice, using sympy for generality and then rewritten for our specific examples using numpy for efficiency.

To better organize the code, we defined a general class which implemented operations such as sampling points, maintaining sets of points, integrating over points, computing geometric tensors

5. This is why this highly nonlinear complex Monge-Ampere equation is relatively tractable. A short derivation is in Headrick and Nassar (2013), and Berndtsson (2013) has an extensive discussion of this point with references.

and the like, hiding details specific to a particular construction of manifolds. We put these details in the `Hypersurface` class. One could write other classes for other manifold definitions, for example hypersurfaces in toric varieties.

Although one might think that the existence of projective coordinates eliminates the need to define coordinate patches, it is better to use them. This is because when we take derivatives in Equation (1), if all of the coordinates are small (as is possible with projective coordinates) we can lose numerical precision and potentially overflow. For example, after taking derivatives Equation (1) of Equation (5), the norm of the coordinates appears in the denominator. This norm depends on the parameters h in Equation (5), and when we go to networks the denominator depends on the weights in an even more complicated way. For numerical stability, it is better to assign the points to patches according to which of their coordinates has the largest magnitude, and then normalize this coordinate to 1. Then, constructing Equation (10) on the hypersurface leads to a second potential division by a small number. This is handled by a further subdivision into subpatches, where a point is assigned to a subpatch according to the largest magnitude of $|\partial f/\partial z^i|$. The class structure `Hypersurface` isolates these details from the rest of the code, which need only know how to deal with several batches of points (coming from the different subpatches). We also implemented a function to generate TensorFlow datasets which store the points on different patches and their patch information. They can be easily loaded and trained as in other neural network problems.

To integrate the code with TensorFlow, we constructed layers which implement Equation (17). Of course we needed a special layer to compute the volume form Equation (7) from the Kähler potential. This requires the computation of the complex hessian $\partial_i \partial_{\bar{j}} K$. With some manipulations, it can be done directly using TensorFlow's backpropagation technique, which allows us to calculate the derivatives efficiently even with higher ks.

In a polynomial network with activation function $z \to z^2$, the weights in the front layers will have higher orders as the depth of the network increases, which will make the values of gradients unstable over each step. To solve this problem, we used the Adam algorithm (Kingma and Ba, 2015) to train our network. It computes an individual adaptive learning rate for each parameter in the network using the first and second moments, which smooths the training process.

Adam and other gradient descent methods are first order, and converge slowly compared with second order methods which use the Hessian. Newton's method is the simplest example. If one starts close to a minimum, a second order method will square the error ϵ with each iteration, and converge very quickly. A rough estimate is that $\epsilon \to \lambda_1 |f'| \epsilon^2$ where λ_1 is the largest eigenvalue of the inverse Hessian $\partial^2 f$.

The inverse Hessian has D^2 components in D dimensions, and it is generally impractical to compute it in a high dimensional parameter space. To deal with this, one can estimate it from the gradient computed at several points. The L-BFGS algorithm (Liu and Nocedal, 1989) does this using the gradients computed in the previous iterations and is often the second order method of choice. It is not much used in practical machine learning, because the signal to noise ratio is generally not high enough to justify high precision optimization, and it is not even available in standard Tensorflow. However it is in an extension package `tensorflow_probability` and it is available in our code.

Another method to solve the exploding/vanishing gradient problem in deep networks is batch normalization (Ioffe and Szegedy, 2015). This is done by standardizing the weights distribution in the training stage, which requires individual recenterings and rescalings of the components in the

vector of sections. This is not allowed in our model, but one could still do a overall rescaling of the vector. We will implement this feature in the future.

4. Results

In the present work we implement the algorithm just proposed, study the dependence of accuracy and speed on the hyperparameters (depth, widths, learning schedule), and propose reasonable values. We intend to study interesting geometry and physics problems elsewhere.

Compared to previous work, the main advantage of this approach is that it can describe arbitrarily complicated metrics with structure on multiple scales. To study this, we considered several quintic CY manifolds with different parameterized families of defining functions $f = 0$. We want to vary the minimal length scale on which the metric will have structure, and we want to scan through geometries with more or less symmetry.

The families we chose were

1. The Dwork quintics $f = 0$ as in Equation (3). Equivalently, $f = f_1$ below with $\phi = 0$.

2. A two parameter family with less symmetry,

$$f_1 = z_0^5 + z_1^5 + z_2^5 + z_3^5 + z_4^5 + \psi z_0 z_1 z_2 z_3 z_4 + \phi(z_3 z_4^4 + z_3^2 z_4^3 + z_3^3 z_4^2 + z_3^4 z_4) \tag{34}$$

3. Another two parameter family,

$$\begin{aligned} f_2 = f_1|_{\phi=0} + \quad \alpha \quad \Big(& z_2 z_0^4 + z_0 z_4 z_1^3 + z_0 z_2 z_3 z_4^2 + z_3^2 z_1^3 + z_4 z_1^2 z_2^2 + z_0 z_1 z_2 z_3^2 + \\ & z_2 z_4 z_3^3 + z_0 z_1^4 + z_0 z_4^2 z_2^2 + z_4^3 z_1^2 + z_0 z_2 z_3^3 + z_3 z_4 z_0^3 + z_1^3 z_4^2 + \\ & z_0 z_2 z_4 z_1^2 + z_1^2 z_3^3 + z_1 z_4^4 + z_1 z_2 z_0^3 + z_2^2 z_4^3 + z_4 z_2^4 + z_1 z_3^4 \Big). \end{aligned} \tag{35}$$

Whereas the Fermat quintic has $\mathbb{Z}_5^4 \times S_5$ discrete symmetry, taking $\psi \neq 0$ breaks this to $\mathbb{Z}_5^3 \times S_5$. The generic CY in the f_1 family has $\mathbb{Z}_5^2 \times S_3$ discrete symmetry, and the generic CY in the f_2 family has no discrete symmetry.[6] Thus specifying their metrics will require successively more data; we will not try to quantify this dependence. We should add that the functions f_1 and f_2 were chosen before beginning our experiments.

A reasonable proxy for the smallest length scale is the distance in the space of defining functions from f to the nearest function f_s which defines a singular Calabi-Yau manifold, one for which $f_s = \nabla f_s = 0$ has a simultaneous solution in $\mathbb{CP}^4$. As we briefly explain in the appendix, this is justified by looking at the generic form of a nearly singular metric and how it depends on the coefficients of f. A suitable definition of the distance is[7]

$$d_{sing}^2(f) = \frac{\min_{Z \in M} \sum_{i=1}^5 \left| \frac{\partial f}{\partial Z^i} \right|^2}{(1/5!) \sum_I (\prod_{i=1}^5 (I_i)!) |f_I|^2} \tag{36}$$

6. We took the parameters ψ, ϕ, α real so there is still a $\mathbb{Z}_2$ complex conjugation symmetry.
7. To clarify the notation in the denominator, a term Z_i^5 in f gets the coefficient $5!/5! = 1$, $Z_1^3 Z_2^2$ gets $3!\dot{2}!/5! = 1/10$, *etc.*.

These values are plotted as heat maps for f_1 in Figure 1(*a*)subfigure and f_2 in Figure 1(*b*)subfigure.

The accuracy of a solution will be measured as the norm of $\eta - 1$ in the L^1 (MAPE), L^2 (RMSE) and L^∞ (MAX) error. In machine learning, one always checks the error twice, for the sample used in optimization (training error) and on another set of points chosen independently (testing error). We followed this practice, in part because it is the default in Tensorflow/Keras, and also to get a conservative error estimate. As we discuss below the difference will be meaningful.

A particular run of the algorithm will depend on various "hyperparameters":

- The depth of the network and width of the layers.
- The number of points N_p for Monte Carlo integrations.
- The batch size N_b for stochastic gradient descent.
- The optimization algorithm and training schedule (number of gradient descent steps, learning rate, *etc.*).

Practically, the most stringent constraints on these parameters are memory limitations. The largest memory items in a network are usually the intermediate results, which for width W are matrices of size $N_b \times W$, with each item taking $4 - 16$ bytes depending on precision and whether complex numbers are needed. Our 32 GB GPUs allowed batches of 100000 points but this was cut to 20000 points for the largest networks (see Table 1).

For a single layer network directly implementing the Fubini-Study metrics Equation (39), W is the total number of parameters. This grows rapidly with k and our memory limited us to $k \leq 4$.[8] By contrast one can run 5 layer and even deeper FNN's.

Out of the networks which can be run, one wants a choice which works robustly (in nearly all cases) with minimal error. Since all metrics of a given k are Fubini-Study metrics , we should compare with the minimal error in this class. Assuming M is nonsingular, this best possible error will decrease exponentially in $k = 2^{\text{depth}}$. As explained in Donaldson (2009) this follows because we are making a polynomial approximation to a C^∞ function. The corresponding statement in Fourier space may be more familiar (the Paley-Wiener theorem).

It is not *a priori* clear to us that this will be the case for our networks. One might hypothesize that the error is controlled instead by the total number of parameters in the network (denote this number as P), the width (as found in Golubeva et al. (2020)), or some other property. So far as we know, work on neural methods for PDE (E and Yu, 2018; Grohs et al., 2019; Müller and Zeinhofer, 2019) has not led to a clear conjecture about this, but it is an interesting question to study.

We next discuss the numbers of total points N_p and batch size N_b. In machine learning, one usually takes $N_b < N_p$ both for computational practicality and to get a noise term in the gradient, parametrically of magnitude $1/\sqrt{N_b}$. Empirically this leads to models which generalize better, for reasons which are not completely sorted out but which include the following. First, ML loss functions are usually non-convex, and noise helps the optimization to escape local minima. This turns out to be the case for our loss functions as well. Second, noise favors finding wide minima (with small second derivatives or even flat directions), and there are statistical arguments that these will generalize better. While our problem is not statistical, since we are using sampling in our

8. With additional programming effort one could probably do $k \leq 6$. By using minibatches one could go higher, but this would require replacing our L-BFGS optimization, perhaps as in Berahas et al. (2016).

computations, this point might be relevant. However we did not find any evidence that decreasing N_b ever improves our results.

A much discussed point in the theory of machine learning is the role of overparameterization. In general, once the number of parameters exceeds the total dimension of the data being fit, one expects to be able to completely fit (interpolate) the data. The optimization problem is easier in this regime, which is a significant advantage. But according to the usual dogma of statistics and of numerical analysis, as one uses more parameters, the extra fitting ability will fit noise, and the accuracy on testing data will decrease. One might have thought that an overparameterized model would not be able to generalize.

Surprisingly, overparameterized models can generalize well. While the reasons for this are still being debated, it seems to be accepted that the dogma we cited is not correct in this regime, with works such as Zhang et al. (2017); Belkin et al. (2019) making many observations which contradict it. It still might be that this paradox can be resolved within current theory. For example, a traditional way to deal with overfitting is to introduce a regularization term in the loss function, such as the sum of the squares of the weights, which favors simpler models (Bishop, 2013). A popular hypothesis is that the choice of initial conditions and optimization algorithm in deep learning produces an implicit regularization term.

Previous works on CY metrics studied highly symmetric metrics with few parameters, so this issue did not arise. But we will encounter this issue, now in a mathematically controlled setting. Thus in §4.2 we also looked at the case $N_p < P$ to see if the situation is similar to that for ML.

4.1. Experiments and Observations

As we explained above, a holomorphic network with width less than the number of sections at a given layer is not able to represent the Fubini-Study metrics at that k, which might lead to problems. In practice we found that these results were very sensitive to the initial conditions for the gradient descent. The bihomogeneous networks were not very sensitive and produced better results, so we restricted the rest of our study to these.

The convergence of some example networks is shown in Figure 2. Adam seems to converge slowly near the minima, so we also introduced a second stage of training using L-BFGS and $N_b = N_p$. This solved the speed problem, converging in a matter of minutes.

To understand the magnitude of the errors, it is useful to estimate the optimal error as a function of k. We did this following an observation of Headrick and Nassar (2013). They found for the Dwork quintics that the error Equation (32) went as $E \propto C^{-k}$, with $C \sim 8$ for the Fermat quintic and varying with ψ. The fit was already good at low k, so by fitting this formula with low values of k, we can estimate the best possible error as a function of k and the parameters of the CY. Thus we optimize over the entire space of metrics Equation (39) for $k = 2, 3, 4$ and do the linear fit

$$\log \text{error} \sim C_0 + C_1 k. \tag{37}$$

This leads to estimated optimal errors, denoted in the plots as `est8` for $k = 8$. We then did sweeps through the parameters of the three families of quintics and compared the results with these optimal errors.

Overall, the network configurations have the largest effect on accuracy. We experimented with networks 50_50_1, 70_70_70_1, 300_300_300_1 and 500_500_500_500_1, etc., corresponding to $k = 4, 8, 16$ with various total number of parameters (see Figure 3, Figure 4 and Table 1). In

general, k plays a more important role here, which agrees with the previous results of Headrick and Nassar (2013): The accuracy of the network models are able to reach approximately the same magnitude as those of the FS models with the corresponding k in all cases, estimated by Equation (37). The dependence on the number of parameters is more complicated. It does not have a significant independent effect for the more symmetric quintics, but it does for those defined by Equation (35), as we discuss in §4.2. For example, the $k = 8$ FS models with 245025 real parameters are predicted to be around a factor of 100 better MSE than $k = 4$. However, the 70_70_70_1 network was able to achieve the same accuracy with only 11620 real parameters for the more symmetric manifolds f_1, and increasing the number of parameters did not seem to improve it. But for f_2, a wider 300_300_300_1 network with 187800 real parameters significantly improved the training accuracy in most cases, although much of this was overfitting (especially for f_1) as one can see in Figure 5(*a*)subfigure.[9] Still, this model was able to attain the FS $k = 8$ accuracy in all cases. While the $k = 8$ FS metrics are simpler than such a network, its memory requirements (at least for a Tensorflow implementation) are challenging, so reproducing its accuracy is of real practical value.

There is also a strong though not exact relation between the distance to the singularity and the error, supporting the idea that the ratio of length scales controlled by this is the dominant parameter. This relation is shown in Figure 3 and Figure 4 and summarized in Table 1, where we quote an average error for "less singular" and "more singular" CYs with distance to the discriminant locus less than (greater than) 0.1. The distance also affects the total number of parameters needed to reach the best accuracy. The 70_70_70_1 network shows similar performance as the 300_300_300_1 one for less singular f_2s (distance greater than 0.15), in comparison to other cases mentioned above.

In scanning through a family of manifolds, training could be made significantly faster by initializing the network with the weights optimized for a nearby parameter value. Details of how to do this and the appropriate learning rates and times can be found in the accompanying software.

For completeness, we also checked the idea that the metrics on the CY manifolds defined by Equation (34) and Equation (35) must be described by non-symmetric models as follows. We computed Kähler metrics using the code developed by Headrick and Nassar (2013), which assumed the discrete symmetry $S_5 \times Z_5^4$, and computed the deviation from Ricci flatness for all three classes of CY defined in §2.2. For $k = 4, 8$ and the symmetric CYs Equation (3), this was roughly the same as for our models. But as one would expect, the errors for Equation (34) and Equation (35) with $\phi, \alpha \neq 0$ were large, of order $0.1 - 0.01$, even for high k.

Some other methods we tested include ℓ_2 regularization, using 64 bit networks and changing loss functions. Most of them did not show a significant impact on our results, but in some cases, it could be helpful to add 0.1*MAX error to the loss function in the early stage of training to prevent getting stuck in a bad local minimum, especially for a deep network and a complicated manifold.

Lastly, we made several attempts to find a model which significantly improves on the performance, including the five layer 300_100_100_100_1 and 500_500_500_500_1 models, and also using the values of the $k = 2$ or $k = 4$ sections as inputs to less deep networks. We found that the optimization was much less robust, often leading to bad local minima. In the second L-BFGS stage, memory limitations restricted us to $N_p \sim 2000$. While some of our runs had up to 10 times better accuracy, these successes were not reliable. Thus for math physics applications we suggest at present using the four layer $N\_N\_N\_1$ networks with $N \sim 100$.

9. This is another motivation to implement minibatched L-BFGS as mentioned in §4.

We believe that further development could improve on this, and our GitHub site will have a benchmark script with a set of test examples and a leaderboard page where we will post new state of the art results.

4.2. More theoretical issues

We turn to discuss theoretical issues for which these results might be relevant. One question we raised earlier is whether the accuracy is controlled more by k or by the number of parameters. While k controls the smallest length scale on which one can vary the metric, it might also be that a complicated metric contains many features at a variety of scales, which require many parameters to represent. Comparing our results for the 70_70_70_1 network and the 300_300_300_1 network suggests that both factors are in play. Whereas both networks attained the maximal accuracy for the simpler and more symmetric hypersurfaces $f_1 = 0$, for the more complicated hypersurfaces $f_2 = 0$ and the more singular cases of these, only the larger network attained this accuracy. This suggests that there is a "complexity" factor which deserves to be quantified and understood.

In theory of ML, the overparameterized regime is usually defined not in terms of an inequality between N_p and P, but rather as the regime in which the model has enough parameters to fit an arbitrary set of N_p observations (Zhang et al., 2017). To locate this threshold in our case, we did runs computing the best $k = 4$ FS metric (with $P = 4900$ parameters) and with a range of N_p values. We found that this model could achieve roughly zero training loss for $N_p \leq 2500$, while the (MSE) testing error had a significant dependence on N_p, consistent with $1/\sqrt{N_p}$. Already for $N_p = 5000$ the training error was comparable to that for larger N_p. Following Zhang et al. (2017), we also trained models with "random labels," here produced by shuffling the η values between the different points, and found the same behavior of training error, along with large testing error. This case can be compared with a random feature model which is solvable in the large N_p, P limit, as we will discuss elsewhere.

5. Conclusions and further directions

We developed and tested software to compute Ricci flat metrics on Calabi-Yau hypersurfaces in projective space. Using it, one can get results with $\sim 0.1\%$ absolute error on CY_3 manifolds with no symmetry. It is based on the standard Tensorflow/Keras platform and can be easily adapted to handle more general Kähler manifolds.

It would be interesting to look at the Laplacian and hermitian Yang-Mills equations and the other applications considered in previous work. Similar techniques could be used to represent other geometries, as we intend to discuss elsewhere.

The Ricci flat Kähler metric problem is one of the better understood problems in nonlinear PDE, with no boundary conditions to complicate the discussion, so it might serve as a good testbed for numerical methods. It would be interesting to try other deep learning PDE methods such as Sirignano and Spiliopoulos (2018). And as we discussed in §4.1, one can get a well motivated estimate for the maximal accuracy which can be obtained for a given depth network. This helps in studying how the accuracy depends on hyperparameters, as we discussed in §4.2. It would be interesting to have more specific theoretical predictions for this dependence.

Acknowledgments

This project was begun in the summer of 2019 at Stony Brook University in collaboration with Tudor Ciobanu. Tudor was a very promising first year graduate student, and his untimely passing fills us with deep sorrow. We hope this work can add to his legacy.

We thank the authors of Anderson et al. (2020) for early discussions and informing us about their work.

We thank Steve Skiena and the Stony Brook AI Institute for the use of their GPU servers.

MRD would like to thank Shing-Tung Yau for discussions, for reading the manuscript and for general support. He thanks Steve Zelditch for discussions on Kähler geometry and comments on Douglas (2020). He also thanks many people for conversations about ML, and especially Sanjeev Arora, David McAllester, Andrea Montanari and Christian Szegedy.

References

Madhu S. Advani, Andrew M. Saxe, and Haim Sompolinsky. High-dimensional dynamics of generalization error in neural networks. *Neural Networks*, 132:428–446, Oct 2020. ISSN 18792782. doi: 10.1016/j.neunet.2020.08.022. URL https://arxiv.org/abs/1710.03667.

Lara B. Anderson, Volker Braun, Robert L. Karp, and Burt A. Ovrut. Numerical Hermitian Yang-Mills connections and vector bundle stability in heterotic theories. *Journal of High Energy Physics*, 2010(6), Apr 2010a. ISSN 11266708. doi: 10.1007/JHEP06(2010)107. URL http://arxiv.org/abs/1004.4399.

Lara B. Anderson, James Gray, Dan Grayson, Yang Hui He, and André Lukas. Yukawa couplings in heterotic compactification. *Communications in Mathematical Physics*, 297(1):95–127, Apr 2010b. ISSN 00103616. doi: 10.1007/s00220-010-1033-8. URL http://arxiv.org/abs/0904.2186.

Lara B. Anderson, Volker Braun, and Burt A. Ovrut. Numerical Hermitian Yang-Mills connections and Kähler cone substructure. *Journal of High Energy Physics*, 2012(1), Mar 2012. ISSN 11266708. doi: 10.1007/JHEP01(2012)014. URL http://arxiv.org/abs/1103.3041.

Lara B. Anderson, Mathis Gerdes, James Gray, Sven Krippendorf, Nikhil Raghuram, and Fabian Ruehle. Moduli-dependent Calabi-Yau and SU(3)-structure metrics from Machine Learning. December 2020. URL https://arxiv.org/abs/2012.04656v1.

Anthony Ashmore. Eigenvalues and eigenforms on Calabi-Yau threefolds. *arXiv:2011.13929 [hep-th]*, November 2020. URL http://arxiv.org/abs/2011.13929. arXiv: 2011.13929.

Anthony Ashmore, Yang Hui He, and Burt A. Ovrut. Machine Learning Calabi–Yau Metrics. *Fortschritte der Physik*, 68(9), Oct 2020. ISSN 15213978. doi: 10.1002/prop.202000068. URL https://arxiv.org/abs/1910.08605.

Paul S. Aspinwall, Tom Bridgeland, Alastair Craw, Michael R. Douglas, Anton Kapustin, Gregory W. Moore, Mark Gross, Graeme Segal, Balázs Szendrői, and P.M.H. Wilson. *Dirichlet branes and mirror symmetry*, volume 4 of *Clay Mathematics Monographs*. AMS, Providence, RI, 2009.

Mikhail Belkin, Daniel Hsu, Siyuan Ma, and Soumik Mandal. Reconciling modern machine-learning practice and the classical bias–variance trade-off. *Proceedings of the National Academy of Sciences of the United States of America*, 116(32):15849–15854, Dec 2019. ISSN 10916490. doi: 10.1073/pnas.1903070116. URL https://arxiv.org/abs/1812.11118.

Albert S. Berahas, Jorge Nocedal, and Martin Takáč. A multi-batch L-BFGS method for machine learning. *Advances in Neural Information Processing Systems*, pages 1063–1071, May 2016. ISSN 10495258. URL http://arxiv.org/abs/1605.06049.

Bo Berndtsson. Convexity on the space of Kähler metrics. *Annales de la faculté des sciences de Toulouse Mathématiques*, 22(4):713–746, 2013. ISSN 0240-2963. doi: 10.5802/afst.1387.

C.M. Bishop. *Pattern Recognition and Machine Learning: All "just the Facts 101" Material*. Information science and statistics. Springer (India) Private Limited, 2013. ISBN 9788132209065.

Lenore Blum, Felipe Cucker, Michael Shub, and Steve Smale. *Complexity and Real Computation*. Springer-Verlag New York, 1 edition, 1998. ISBN 978-0-387-98281-6. doi: 10.1007/978-1-4612-0701-6.

Volker Braun, Tamaz Brelidze, Michael R. Douglas, and Burt A. Ovrut. Eigenvalues and eigenfunctions of the scalar Laplace operator on Calabi-Yau manifolds. *Journal of High Energy Physics*, 2008(7), May 2008a. ISSN 11266708. doi: 10.1088/1126-6708/2008/07/120. URL http://arxiv.org/abs/0805.3689.

Volker Braun, Tamaz Brelidze, Michael R. Douglas, and Burt A. Ovrut. Calabi-Yau metrics for quotients and complete intersections. *Journal of High Energy Physics*, 2008(5), Dec 2008b. ISSN 11266708. doi: 10.1088/1126-6708/2008/05/080. URL http://arxiv.org/abs/0712.3563.

R S Bunch and Simon K Donaldson. Numerical approximations to extremal metrics on toric surfaces. *Handbook of geometric analysis. {N}o. 1*, 7:1–28, Mar 2008. URL http://arxiv.org/abs/0803.0987.

Philip Candelas and Xenia C. de la Ossa. Comments on conifolds. *Nuclear Physics, Section B*, 342 (1):246–268, 1990. ISSN 05503213. doi: 10.1016/0550-3213(90)90577-Z.

Philip Candelas, Xenia C. de la Ossa, Paul S. Green, and Linda Parkes. An exactly soluble superconformal theory from a mirror pair of Calabi-Yau manifolds. *Physics Letters B*, 258(1-2): 118–126, 1991. ISSN 03702693. doi: 10.1016/0370-2693(91)91218-K.

Grigorios G. Chrysos, Stylianos Moschoglou, Giorgos Bouritsas, Yannis Panagakis, Jiankang Deng, and Stefanos Zafeiriou. $\Pi-$nets: Deep polynomial neural networks. *Proceedings of the IEEE Computer Society Conference on Computer Vision and Pattern Recognition*, pages 7323–7333, Mar 2020. ISSN 10636919. doi: 10.1109/CVPR42600.2020.00735. URL https://arxiv.org/abs/2003.03828.

Wei Cui and James Gray. Numerical metrics, curvature expansions and Calabi-Yau manifolds. *Journal of High Energy Physics*, 2020(5):1568–1575, Dec 2020. ISSN 10298479. doi: 10.1007/JHEP05(2020)044. URL https://arxiv.org/abs/1912.11068.

G. Cybenko. Approximation by superpositions of a sigmoidal function. *Mathematics of Control, Signals, and Systems*, 2(4):303–314, 1989. ISSN 09324194. doi: 10.1007/BF02551274.

S. K. Donaldson. Some numerical results in complex differential geometry. *Pure and Applied Mathematics Quarterly*, 5(2):571–618, Dec 2009. ISSN 15588602. doi: 10.4310/PAMQ.2009.v5.n2.a2. URL https://arxiv.org/abs/math/0512625.

Charles Doran, Matthew Headrick, Christopher P. Herzog, Joshua Kantor, and Toby Wiseman. Numerical Kähler-Einstein metric on the third del Pezzo. *Communications in Mathematical Physics*, 282(2):357–393, Mar 2008. ISSN 00103616. doi: 10.1007/s00220-008-0558-6. URL https://arxiv.org/abs/hep-th/0703057.

Michael R. Douglas. Calabi-Yau metrics and string compactification. *Nuclear Physics B*, 898: 667–674, Mar 2015. ISSN 05503213. doi: 10.1016/j.nuclphysb.2015.04.009. URL https://arxiv.org/abs/1503.02899.

Michael R. Douglas. Holomorphic feedforward networks. 2020. To appear in the Pure and Applied Mathematics Quarterly special issue in honor of Professor Bernie Shiffman.

Michael R. Douglas, Robert L. Karp, Sergio Lukic, and René Reinbacher. Numerical solution to the hermitian Yang-Mills equation on the Fermat quintic. *Journal of High Energy Physics*, 2007(12):083–083, Dec 2007. ISSN 1029-8479. doi: 10.1088/1126-6708/2007/12/083. URL https://arxiv.org/abs/hep-th/0606261.

Michael R. Douglas, Robert L. Karp, Sergio Lukic, and Reń Reinbacher. Numerical Calabi-Yau metrics. *Journal of Mathematical Physics*, 49(3), Dec 2008. ISSN 00222488. doi: 10.1063/1.2888403. URL http://arxiv.org/abs/hep-th/0612075.

Weinan E and Bing Yu. The Deep Ritz Method: A Deep Learning-Based Numerical Algorithm for Solving Variational Problems. *Communications in Mathematics and Statistics*, 6(1), Sep 2018. ISSN 2194671X. doi: 10.1007/s40304-018-0127-z. URL https://arxiv.org/abs/1710.00211.

Davide Gaiotto, Gregory W. Moore, and Andrew Neitzke. Four-dimensional wall-crossing via three-dimensional field theory. *Communications in Mathematical Physics*, 299(1):163–224, Jul 2010. ISSN 00103616. doi: 10.1007/s00220-010-1071-2. URL https://arxiv.org/abs/0807.4723.

Anna Golubeva, Behnam Neyshabur, and Guy Gur-Ari. Are wider nets better given the same number of parameters? Oct 2020. URL http://arxiv.org/abs/2010.14495.

Ian Goodfellow, Yoshua Bengio, and Aaron Courville. *Deep Learning*. MIT Press, 2016. http://www.deeplearningbook.org.

P. Griffiths and J. Harris. *Principles of Algebraic Geometry*. Wiley Classics Library. Wiley, 2014. ISBN 9781118626320.

Philipp Grohs, Fabian Hornung, Arnulf Jentzen, and Philipp Zimmermann. Space-time error estimates for deep neural network approximations for differential equations. *arXiv*, Aug 2019. URL https://arxiv.org/abs/1908.03833.

Matthew Headrick and Ali Nassar. Energy functionals for Calabi-Yau metrics. *Advances in Theoretical and Mathematical Physics*, 17(5):867–902, Aug 2013. ISSN 10950753. doi: 10.4310/ATMP.2013.v17.n5.a1. URL https://arxiv.org/abs/0908.2635.

Matthew Headrick and Toby Wiseman. Numerical ricci-flat metrics on K3. *Classical and Quantum Gravity*, 22(23):4931–4960, Jun 2005. ISSN 02649381. doi: 10.1088/0264-9381/22/23/002. URL http://arxiv.org/abs/hep-th/0506129.

Kentaro Hori, Sheldon Katz, Albrecht Klemm, Rahul Pandharipande, Richard Thomas, Cumrun Vafa, Ravi Vakil, and Eric Zaslow. *Mirror symmetry*, volume 1 of *Clay Mathematics Monographs*. American Mathematical Society, Providence, RI; Clay Mathematics Institute, Cambridge, MA, 2003. ISBN 0-8218-2955-6. With a preface by Vafa.

Stephan Hoyer, Jascha Sohl-Dickstein, and Sam Greydanus. Neural reparameterization improves structural optimization. *arXiv*, Sep 2019. URL https://arxiv.org/abs/1909.04240.

D. Huybrechts. *Complex Geometry: An Introduction*. Universitext (Berlin. Print). Springer, 2005. ISBN 9783540212904.

Sergey Ioffe and Christian Szegedy. Batch normalization: Accelerating deep network training by reducing internal covariate shift. *32nd International Conference on Machine Learning, ICML 2015*, 1:448–456, Feb 2015. URL http://arxiv.org/abs/1502.03167.

Shamit Kachru, Arnav Tripathy, and Max Zimet. K3 metrics. Jun 2020. URL http://arxiv.org/abs/2006.02435.

Taehwan Kim and Tülay Adalı. Approximation by fully complex multilayer perceptrons. *Neural computation*, 15(7):1641–1666, 2003.

Diederik P. Kingma and Jimmy Lei Ba. Adam: A method for stochastic optimization. *3rd International Conference on Learning Representations, ICLR 2015 - Conference Track Proceedings*, Dec 2015. URL https://arxiv.org/abs/1412.6980.

D. C. Liu and J. Nocedal. On the limited memory BFGS method for large scale optimization. *Mathematical Programming*, 45:503–528, 1989. URL https://link.springer.com/content/pdf/10.1007{%}2FBF01589116.pdf.

Stefano Sarao Mannelli, Eric Vanden-Eijnden, and Lenka Zdeborová. Optimization and Generalization of Shallow Neural Networks with Quadratic Activation Functions. Jun 2020. URL http://arxiv.org/abs/2006.15459.

Johannes Müller and Marius Zeinhofer. Deep Ritz Revisited. *arXiv*, Dec 2019. URL https://arxiv.org/abs/1912.03937.

Reza Seyyedali. Numerical algorithm for finding balanced metrics on vector bundles. *Asian Journal of Mathematics*, 13(3):311–322, Apr 2009. ISSN 10936106. doi: 10.4310/AJM.2009.v13.n3.a3. URL http://arxiv.org/abs/0804.4005.

Bernard Shiffman and Steve Zelditch. Distribution of zeros of random and quantum chaotic sections of positive line bundles. *Communications in Mathematical Physics*, 200(3):661–683, Mar 1999. ISSN 00103616. doi: 10.1007/s002200050544. URL https://arxiv.org/abs/math/9803052.

Justin Sirignano and Konstantinos Spiliopoulos. Dgm: A deep learning algorithm for solving partial differential equations. *Journal of computational physics*, 375:1339–1364, 2018.

Felix Voigtlaender. The universal approximation theorem for complex-valued neural networks. *arXiv:2012.03351 [cs, math, stat]*, December 2020. URL http://arxiv.org/abs/2012.03351. arXiv: 2012.03351.

Chiyuan Zhang, Benjamin Recht, Samy Bengio, Moritz Hardt, and Oriol Vinyals. Understanding deep learning requires rethinking generalization. *5th International Conference on Learning Representations, ICLR 2017 - Conference Track Proceedings*, Nov 2017. URL http://arxiv.org/abs/1611.03530.

Appendix A. Plots and tables

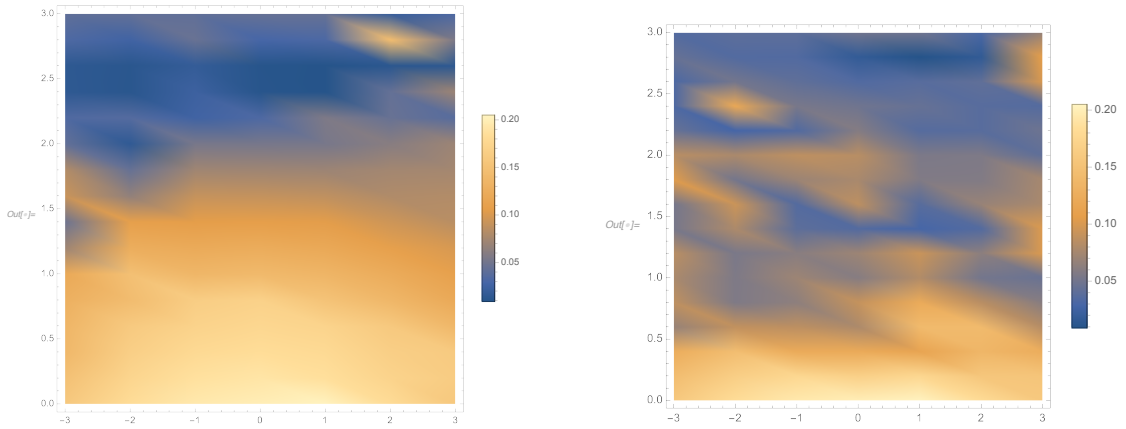

(*a*) (*b*)

Figure 1: Distance to singular CY as function of ψ, ϕ in Equation (34) (Left) and ψ, α in Equation (35) (Right)

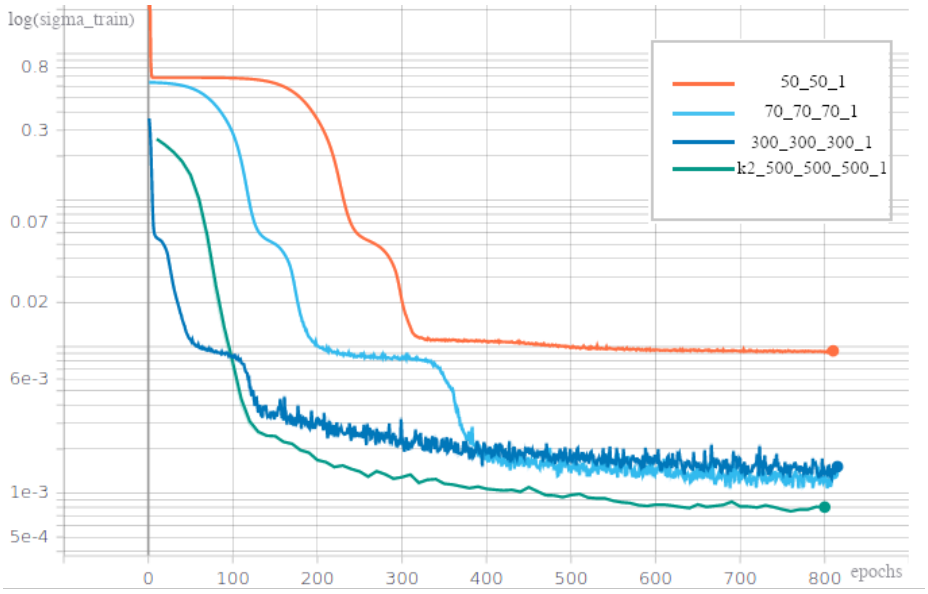

Figure 2: The training curves for Equation (3) with $\psi = 0.5$, trained with Adam optimizer and MAPE loss. The data for k2_500_500_500_1 was recorded every 10 epochs.

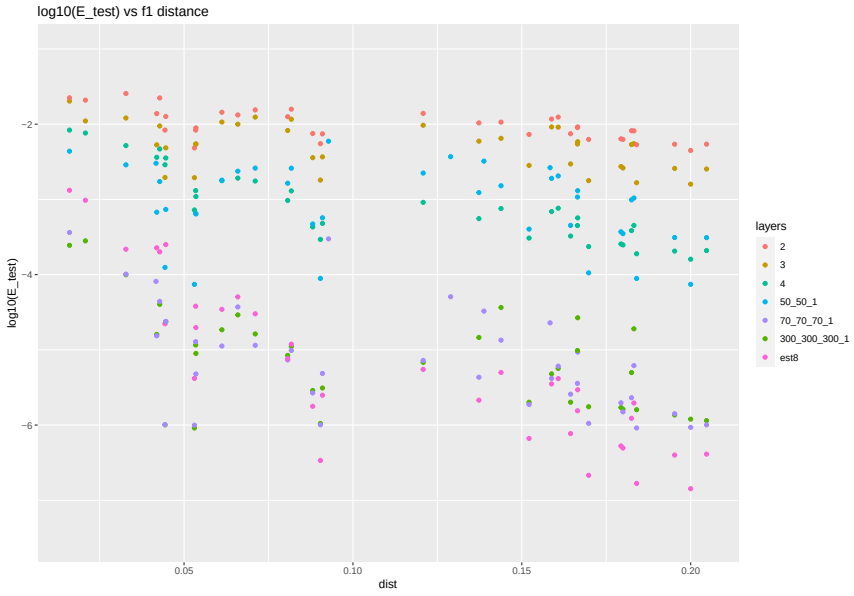

Figure 3: Mean testing $(\eta - 1)^2$ function of d_{sing} in f1 Equation (34) with k = 2, 3, 4, the extrapolated k = 8, and three neural network models

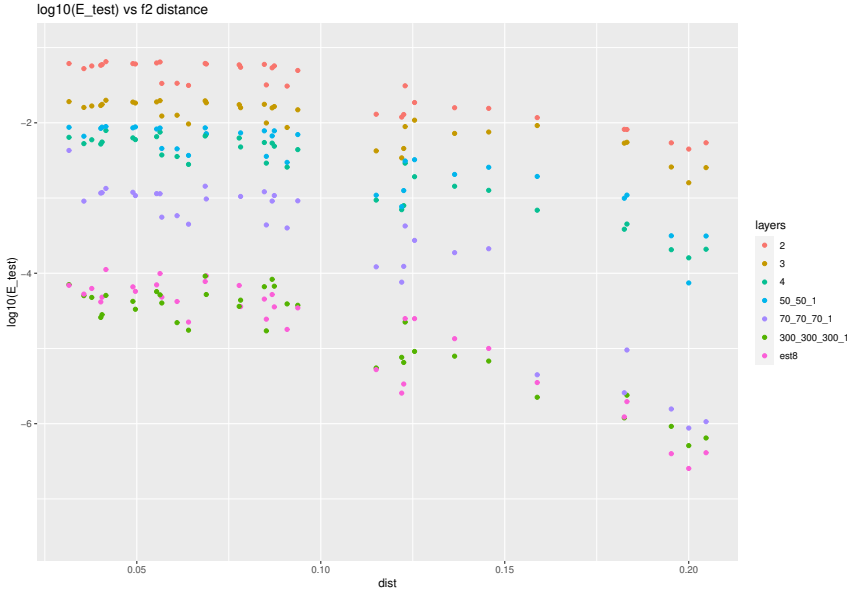

Figure 4: Mean testing $(\eta - 1)^2$ function of d_{sing} in f2 Equation (35) with k = 2, 3, 4, the extrapolated k = 8, and three neural network model

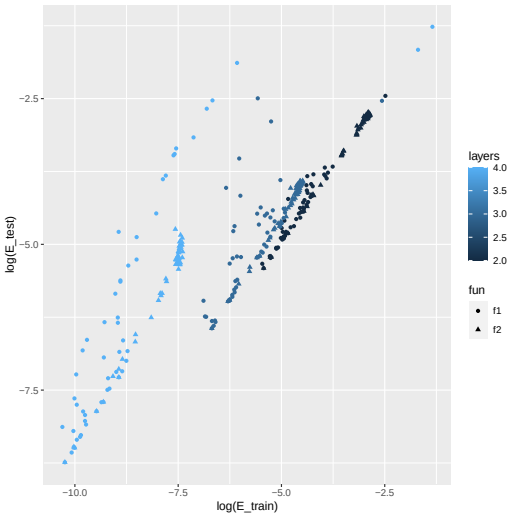

(*a*) log(E_test) vs log(E_train) with L-BFGS

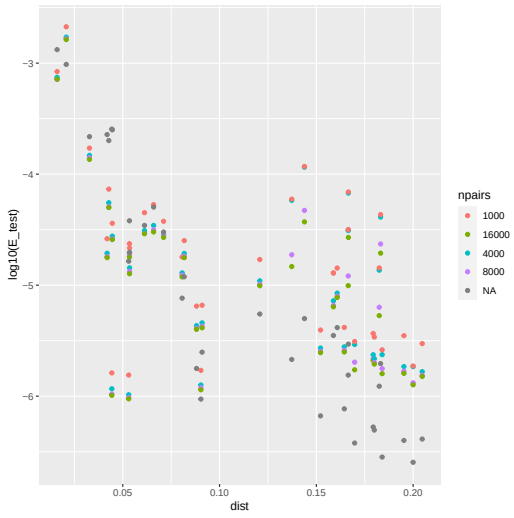

(*b*) f1 log(E_test) vs dist for 300_300_300_1, L-BFGS and different numbers of point groups (each with five points). The "NA" entry is the extrapolated FS accuracy at $k = 8$.

Figure 5: The overparameterization of L-BFGS

Table 1: A summary of the average $\log_{10}$(E_train) and $\log_{10}$(E_train) over runs of different distances

func	distance	layers	n_params	n_pts_lbfgs	$\langle\log_{10}(\text{E\_train})\rangle$	$\langle\log_{10}(\text{E\_test})\rangle$
f1	<0.1	50_50_1	3800	100000	-3.07	-3.00
f1	>=0.1	50_50_1	3800	100000	-3.17	-3.14
f1	<0.1	70_70_70_1	11620	100000	-5.02	-4.86
f1	>=0.1	70_70_70_1	11620	100000	-5.45	-5.40
f1	<0.1	300_300_300_1	187800	80000	-5.94	-4.89
f1	>=0.1	300_300_300_1	187800	80000	-5.78	-5.38
f2	<0.1	50_50_1	3800	100000	-2.22	-2.18
f2	>=0.1	50_50_1	3800	100000	-3.03	-3.01
f2	<0.1	70_70_70_1	11620	100000	-3.15	-3.01
f2	>=0.1	70_70_70_1	11620	100000	-4.68	-4.62
f2	<0.1	300_300_300_1	187800	20000	-5.86	-4.37
f2	>=0.1	300_300_300_1	187800	20000	-6.11	-5.48

Appendix B. Reviews of the concepts

B.1. Complex and Kähler geometry

This is a very brief introduction meant for readers familiar with real differential geometry and the concepts of manifolds, tensor fields, differential forms, Riemannian metrics, and curvature.

A complex manifold M is a topological space which is locally similar to the d-dimensional space $\mathbb{C}^d$. One can define it in terms of coordinate patches U_α whose union is M, and coordinate maps Z_α which are complex diffeomorphisms between U_α and a contractible subset of $\mathbb{C}^d$. As a linear space, $\mathbb{C}^d \cong \mathbb{R}^{2d}$, with coordinates $Z^i = X^i + iY^i$, and thus every complex manifold is also a real manifold. But the complex coordinate systems provide additional structure, summarized by a linear operator J_x at each point $x \in M$, which turns a tangent vector corresponding to a small motion in the $\mathrm{Re}Z^i$ direction (and corresponding to $\partial/\partial \mathrm{Re}Z^i$) into the vector corresponding to $\mathrm{Im}Z^i$. These operators combine to a linear tensor operator which maps the tangent space $TM \to TM$, and can be denoted in tensor notation as J^i_j. Complex geometry can also be phrased as a "special geometry" in which operations such as the covariant derivative preserve the complex structure, so $\nabla_i J^k_l = 0$. From this point of view, all of the concepts of real geometry we listed above have the same primary definitions in complex geometry, but they satisfy additional constraints.

In complex geometry one often uses the "bar" notation for complex conjugation and tensors. Complex conjugate coordinates are denoted $(Z^i)^*$ or interchangeably $\bar{Z}^{\bar{j}}$. Thus, a tangent space T_xM is a direct sum of a complex tangent space $T_{\mathbb{C},x}M$ with coordinate basis $(\partial/\partial Z^1, \ldots, \partial/\partial Z^d)$ and a complex conjugate tangent space with coordinate basis $(\partial/\partial \bar{Z}^1, \ldots, \partial/\partial \bar{Z}^d)$. Here $\partial/\partial Z^i = \frac{1}{2}(\partial/\partial X^i - i\partial/\partial Y^i)$, with the constant chosen so that $\partial Z^j/\partial Z^i = \delta^j_i$. We have $\partial Z^j/\partial \bar{Z}^i = 0$ and a holomorphic function f is defined as one for which $\partial f/\partial \bar{Z}^i = 0 \, \forall i$, generalizing the definition in one complex dimension.

The Euclidean metric $ds^2 = (dX^1)^2 + (dY^1)^2 + \ldots + (dX^d)^2 + (dY^d)^2$ becomes $ds^2 = dZ^1 d\bar{Z}^1 + \ldots + dZ^d d\bar{Z}^d$, This is written in tensor notation as $ds^2 = g_{i\bar{j}} dZ^i d\bar{Z}^{\bar{j}}$ with $g_{i\bar{j}} \equiv \delta_{i,\bar{j}}$ with components 1 if the indices agree ($i = \bar{j}$) and zero otherwise. A general Riemannian metric can be written in this notation and could also have terms $g_{ij} dZ^i dZ^j$, $g_{\bar{i}\bar{j}} d\bar{Z}^{\bar{i}} d\bar{Z}^{\bar{j}}$ and $g_{\bar{i}j} d\bar{Z}^{\bar{i}} dZ^j$. But we will only consider hermitian metrics, for which the metric tensor is a positive definite hermitian matrix. In complex notation this requires $g_{ij} = g_{\bar{i}\bar{j}} = 0$ and $g_{\bar{i}j} = g^*_{i\bar{j}}$.

After $\mathbb{C}^d$, the next simplest example of a complex manifold is complex projective space $\mathbb{CP}^d$. This can be defined in terms of patches, but the shortest and clearest definition is as a quotient $\mathbb{CP}^d \equiv \{\mathbb{C}^{d+1} - \mathbf{0}\}/\sim$. Let the complex coordinates of $\mathbb{C}^{d+1}$ be $(Z^1, Z^2, \ldots, Z^{d+1})$, then $(Z^1, Z^2, \ldots, Z^{d+1}) \sim (\lambda Z^1, \lambda Z^2, \ldots, \lambda Z^{d+1})$ for every $\lambda \in \{\mathbb{C} - 0\}$. One can cover $\mathbb{CP}^d$ by coordinate charts U_α, where U_α is defined by choosing the representative of $\sim$ in which $Z^\alpha = 1$. The space $\mathbb{CP}^1$ is topologically identical to S^2. It is $\mathbb{C}$ with an additional point at "infinity," or the Riemann sphere. The cases $d > 1$ are not homeomorphic to spheres. Like the spheres, each complex projective space has a maximally symmetric metric, called the Fubini-Study metric. For $\mathbb{CP}^1$ it is isomorphic to the usual round metric on S^2.

This metric is best defined by first defining the more general concept of Kähler metric. This is a metric which locally (so, in each patch U_α) is the second derivative of a real function K_α on U_α,

$$g_{i\bar{j}} = \frac{\partial^2}{\partial Z^i \partial \bar{Z}^{\bar{j}}} K_\alpha. \tag{38}$$

The Kähler potential for the Euclidean metric on $\mathbb{C}^d$ is $K = \sum_i |Z^i|^2$. These metrics are hermitian, but have many further special properties and simplifications.

Now, the Fubini-Study metric on $\mathbb{CP}^d$ can be defined by the Kähler potential

$$K = \log \sum_{i,\bar{j}=1}^{d+1} h_{i\bar{j}} Z^i \bar{Z}^{\bar{j}}, \tag{39}$$

where h is a $(d+1)\times(d+1)$ positive definite hermitian matrix h. Note that this is not a function on $\mathbb{CP}^d$, because it is not invariant under the equivalence relation $\boldsymbol{Z} \sim \lambda \boldsymbol{Z}$. However since it changes by addition of a term whose second derivative Equation (38) vanishes, it defines a metric on $\mathbb{CP}^d$. One can also think of this as specifying a different (yet compatible) function in each patch U_α. One gets the same metric on $\mathbb{CP}^d$ for any choice of h. This is because one can always find a linear change of coordinates $Z^i \to L^i_j Z^j$ which turns h into the identity matrix. Thus one usually speaks of "the" Fubini-Study metric on $\mathbb{CP}^d$.

The main object of our studies here will be hypersurfaces in $\mathbb{CP}^d$. A hypersurface in $\mathbb{C}^{d+1}$ is the set of solutions to an equation $f = 0$, as in Equation (3). If f is a homogeneous polynomial, the quotient by the relation $\sim$ above also makes sense for the hypersurface, thus defining a hypersurface in $\mathbb{CP}^d$, which is a $d-1$-dimensional manifold if the condition Equation (4) is satisfied at each point. While this construction only produces a small subset of the possible complex manifolds, these already exhibit a great diversity of behavior. The specific choice in Equation (3) was made to get manifolds with Ricci flat metrics, as explained in the literature.

As in real geometry, given a map $M \to N$, one can pull back a metric on N to get a metric on M. One can check that for Kähler geometry, this can be done by first restricting the Kähler potential K from N to M and then applying Equation (38) on M. To relate derivatives on M to derivatives on N, one uses $\partial_i f|_M = 0$ to solve for one component of $\partial_i|_N$ in terms of the others. This defines a projection matrix such that $\partial_i|_M = L^{i'}_i \partial_{i'}|_N$,

$$L^{i'}_i = \begin{cases} \delta^{i'}_i, & 1 \le i, i' \le n, \\ -(\partial f/\partial Z^i)/(\partial f/\partial Z^{n+1}), & i' = n+1 \end{cases} \tag{40}$$

Thus we can regard Equation (39) as defining a family of metrics on a hypersurface, depending on the $(d+1)^2$ real parameters of h. Whereas these were equivalent on $\mathbb{CP}^d$, since the linear transformation $Z^i \to L^i_j Z^j$ will generally not preserve the function f, these metrics are generally distinct on M. This gives us a parameterized family of metrics on M, but of too low dimension for our purposes. The next subsection will explain how we can get larger families.

While we will not review curvature in detail, the formulas which determine the connection and curvature in terms of the metric are much simpler in Kähler geometry. We quote the Ricci curvature,

$$R_{i\bar{j}} = \frac{\partial^2}{\partial Z^i \bar{\partial} \bar{Z}^{\bar{j}}} \log \det_{i,\bar{j}} g_{i\bar{j}}, \tag{41}$$

which can be used to justify Equation (7).

B.2. Line bundles and the embedding method

Following Donaldson (2009), most work on numerical Calabi-Yau metrics represents the metric using an embedding by holomorphic sections of a very ample line bundle $\mathcal{L}$. This embedding is

a map into a linear space, analogous to spectral embeddings such as the "Laplacian eigenmap" construction, but with the great advantage that the map has a simple exact form. Let us briefly review it.

A section of a holomorphic line bundle is locally a holomorphic function. To define it globally, we define the line bundle by choosing patches U_α on the manifold M and holomorphic transition functions $f_{\alpha\beta}$ on the overlaps of patches $U_\alpha \cup U_\beta$ satisfying the consistency conditions $f_{\alpha\beta} f_{\beta\gamma} f_{\gamma\alpha} = 1$. A section s is then a holomorphic function s_α on each patch satisfying $s_\alpha = f_{\alpha\beta} s_\beta$. Now this is ambiguous considered as a function, because we can always multiply by a set of holomorphic functions λ_α defined on each patch, taking $s_\alpha \to \lambda_\alpha s_\alpha$. But the ratio of a pair of sections is unambiguous. This can be rephrased as the statement that a vector of N sections is an unambiguous map ι from M to $\mathbb{CP}^{N-1}$, since λ_α acts to rescale the entire vector. The very ample condition then states that the map ι is an embedding.

Consider the quintic hypersurface defined by Equation (3). In this case, one can show that all holomorphic line bundles extend to the ambient space $\mathbb{CP}^4$. These are parameterized by an integer k and denoted $\mathcal{O}_{\mathbb{CP}^4}(k)$. For $k \geq 0$ they have holomorphic sections, which are precisely the homogeneous polynomials of degree k in the coordinates Z^i. These form a linear space which is denoted $H^0(\mathcal{O}_{\mathbb{CP}^4}(k))$. Take $k = 1$ for example. $H^0(\mathcal{O}_{\mathbb{CP}^4}(1))$ is the space of linear polynomials in the homogeneous coordinates Z^i. Its dimension, denoted $h^0(\mathcal{O}_{\mathbb{CP}^4}(1))$, is 5. Similarly $h^0(\mathcal{O}_{\mathbb{CP}^4}(k)) = \binom{k+4}{k}$.

Because a section is locally just a function, it can be restricted to a submanifold, thus defining the bundles $\mathcal{O}_M(k)$. This map is not injective – a section proportional to the defining polynomial f will restrict to zero. This is nontrivial for $k \geq 5$ – for example for $\mathcal{O}_M(5)$, the sections are fifth degree polynomials with a single redundancy: if we add f to the section with an arbitrary coefficient, since $f = 0$ on M, we do not change the section. To get a complete and nonredundant basis, one needs to take this into account. But since our neural networks will generate spaces of sections which are not complete and can be redundant, we will not bother to take this quotient.

In general, the representation of a manifold by an embedding has advantages and disadvantages. Two disadvantages are that it can be hard to construct explicit coordinate charts, and the embedding is an additional structure which may or may not be well suited to the problem at hand. In our case, we will not need explicit coordinate charts; the only global operation we will need is to do integrals on M, and this can be done by Monte Carlo (sampling points), as in Douglas et al. (2008).

The second problem is mitigated if one can find a canonical embedding, determined by the intrinsic geometry of M and not involving other choices. This is indeed the case here: if we use a complete basis of sections, which we can do because the basis is finite dimensional, the embedding depends only on the choice of line bundle.

The embedding representation gives us a natural family of metrics: we choose a family of metrics on the embedding space, and the pullback to M gives us a family on M. For an embedding in $\mathbb{R}^N$, we could take the Euclidean metrics $g_{ij} dx^i dx^j$ parameterized by a symmetric matrix g_{ij}. While on $\mathbb{R}^N$ these are all related by linear change of coordinates, once we pull back to M this generally provides a family of distinct metrics.

In the case at hand, the natural family of Kähler metrics is the family of Fubini-Study metrics on complex projective space. As we discussed in Appendix B.1, using the original ambient space $\mathbb{CP}^4$ gives us a family of metrics but of low dimension. This problem is now solved. Using our embedding by a basis of N sections s^I, and pulling back the Fubini-Study metric on $\mathbb{CP}^{N-1}$, the

embedding then leads to the Kähler potential

$$K = \log \sum_{I,\bar{J}} h_{I,\bar{J}} s^I \bar{s}^{\bar{j}} \tag{42}$$

where s^I is a basis of $N = h_0(\mathcal{L})$ holomorphic sections. This gives us an N^2 real dimensional family of metrics parameterized by the hermitian matrix $h_{I,\bar{J}}$.

B.3. Feed-forward networks

Let us briefly review the definition of a feed-forward network (FFN, also called MLP for multilayer perceptron). It is a parameterized function

$$F_w : \mathcal{X} \to \mathcal{Y}, \tag{43}$$

with an input $x \in \mathcal{X} \cong \mathbb{R}^D$ and an output $y \in \mathcal{Y} \cong \mathbb{R}^{D'}$ (we will generally take $D' = 1$). We can define it as the composition of a series of functions

$$F_w = W^{(d)} \circ \theta \circ W^{(d-1)} \circ \ldots \circ \theta \circ W^{(1)} \circ \theta \circ W^{(0)}, \tag{44}$$

where the $W^{(i)}$'s are general linear transformations, and θ is a nonlinear function which acts independently on each vector component. Explicitly,

$$W^{(i)} : \mathbb{R}^{D_i} \to \mathbb{R}^{D_{i+1}} : v \to W^{(i)} v \tag{45}$$

where the $W^{(i)}$ on the right is a rectangular matrix, $D_0 = D, D_{d+1} = D'$ and the dimensions $D_1, D_2, \ldots$ of the intermediate vector spaces can be freely chosen. The function θ can be written as a sum over a basis e_a as

$$\theta : \mathbb{R}^{D_i} \to \mathbb{R}^{D_i} : v \to \sum_{a=1}^{D_i} e_a \theta(v_a) \tag{46}$$

where the $\theta(x)$ on the right, called the "activation function," maps $\mathbb{R} \to \mathbb{R}$. Two popular choices are $\theta(x) = \tanh x$, and the "ReLU" function

$$\theta_{ReLU}(x) = \begin{cases} x, x \geq 0 \\ 0, x < 0 \end{cases} . \tag{47}$$

One generally refers to a combination $\theta \odot W$ as a layer, with the final layer $W^{(d)}$ being an exception in not having θ. The term "unit" is sometimes used to denote the computation which takes an input v and produces a single component of $(\theta \circ W)(v)$, so this network will have $D_1 + \ldots + D_d$ units. The number of layers $d + 1$ is the depth.

It has been shown that feed-forward networks can approximate arbitrary functions, including complex functions Voigtlaender (2020); Kim and Adalı (2003). This is the case even for depth two ($d = 1$) (Cybenko, 1989), but in this case one can need an exponentially large number of units, as would be the case for simpler methods of interpolation (the "curse of dimension"). By using more layers, one can gain many advantages – complicated functions can be represented with many fewer units, and local optimization techniques are much more effective. How exactly this works is not well understood theoretically and there are many interesting observations and hypotheses as to how these advantages arise.

B.4. Supervised learning, sampling and data

In supervised learning, we have a data set of N_{data} items, each of which is an input-output pair (x_n, y_n). These are supposed to be drawn from a probability distribution $\mathcal{P}$ on $\mathcal{X} \times \mathcal{Y}$. The goal is to choose the function Equation (43) from $\mathcal{X}$ to $\mathcal{Y}$ which best describes the general relation $\mathcal{P}$ between input and output, in the sense that it minimizes some definition of the expected error (an objective or "loss" function). The procedure of making this choice given the data set is called training the network.

A simple choice of objective function is the mean squared error (MSE),

$$\mathcal{E} = \mathbb{E}_{\mathcal{P}}\left[(f_w(x) - y)^2\right]. \tag{48}$$

If we estimate this by evaluating it on our data set, we get the training error

$$\mathcal{E}_{train} = \frac{1}{N_{data}} \sum_{n=1}^{N_{data}} (f_w(x_n) - y_n)^2. \tag{49}$$

Alternatively, one can also use the mean absolute percentage error (MAPE),

$$\mathcal{E} = \mathbb{E}_{\mathcal{P}}\left[\frac{|f_w(x) - y|}{y}\right]. \tag{50}$$

A standard ML training procedure is the following. We start with an MLP as in Equation (15), with the weights initialized to random values – in other words, we draw the w from some distribution independent of the data. A common choice is for each matrix element $w_{i_m}^{(m),i_{m+1}}$ to be an independent Gaussian random variable with mean zero and variance $1/\sqrt{D_m}$. This choice is made so that the expected eigenvalues of the weight matrix remain order one as we vary the D_m's.

The next step is to minimize Equation (49) as a function of the weights. A simple algorithm for this is gradient descent, a stepwise process in which the weights at time $t+1$ are derived from those at t as

$$w(t+1) = w(t) - \epsilon(t) \frac{\partial \mathcal{E}_{train}}{\partial w}\bigg|_{w=w(t)}. \tag{51}$$

While this will only find a local minimum, it works better for these problems than one might have thought. One trick for improving the quality of the result is to make the step size $\epsilon(t)$ decrease with time, according to a "learning schedule" chosen empirically to get good results for the task at hand.

A variation on this procedure is "stochastic gradient descent" or SGD. This is much like Equation (51) except that instead of evaluating the training error $\mathcal{E}_{train}$ on the full data set, one evaluates it on a subset (or "batch") of the data set, with the batch varied from one step to the next so that their union covers the full data set. This was originally done for computational reasons but it also turns out to produce a noise term with beneficial properties, for example in helping to escape local minima. There are also many variations on SGD as well as other optimization algorithms, each with advantages for certain applications. We will describe our methods in §3.2.

Once the optimization is deemed to have converged, one judges the results by estimating Equation (48). This estimate must be made by using an independent data set from that used in training as otherwise we are rewarding our model for matching both signal and noise.[10] However in most

10. In classification problems, one often uses networks with many more parameters than data points and which can completely fit the dataset, so that the minimum of $\mathcal{E}_{train}$ is zero! In this case $\mathcal{E}_{train}$ is clearly a poor estimate for $\mathcal{E}$.

applications we do not have any direct access to $\mathcal{P}$, rather we only have an empirical data set. Thus one starts by dividing the full data set into disjoint "training" and "testing" subsets, evaluates Equation (49) on the training set for training, and then evaluates the sum of errors over the testing set to estimate $\mathcal{E}$. The final model can be very accurate, surprisingly so when compared to expectations from standard statistical theory. Let us cite Zhang et al. (2017); Belkin et al. (2019) as two influential recent papers which developed this point.

While our problem is not one of supervised learning, it will be useful to phrase it in terms as similar as possible, so that we can most easily use ML software. The workflow of the supervised learning task involves defining a set of data points (x_n, y_n) which are independent of the weights, repeated evaluation of the network at each x_n to get a prediction $f(x_n)$ for the corresponding y_n, and optimization of an objective function which is a sum of terms which each depend on a single data point. The network is normally defined by concatenating layers, such as multiplication by a weight matrix (a fully connected layer), application of an activation function, and so on. These layers are implemented in associated software libraries, such as Keras for Tensorflow. As we explain in §3.1, while we will have to implement some new layers for our problem, otherwise our workflow is the same.

Appendix C. Nearly singular Calabi-Yau threefolds

As discussed in the main text, a hypersurface M defined as the solutions to $f = 0$ will be a manifold only if $\partial f = 0$ everywhere on M. There is much to say about the singular case, but our computations will be for non-singular manifolds. Still, a manifold which is nearly singular in the sense we now describe will have small cycles and a Ricci flat metric with corresponding large ratio of length scales, which is the leading effect controlling the accuracy of our numerical metrics. Here we give a heuristic discussion of this dependence.

The generic singularity of a hypersurface is an ordinary double point (ODP). In a small neighborhood of a $D = 3$ ODP singularity it looks like

$$z_1^2 + z_2^2 + z_3^2 + z_4^2 = \epsilon \tag{52}$$

and the singular limit is $\epsilon \to 0$. This is usually called the conifold singularity in the string theory literature. A Ricci-flat metric on this noncompact manifold is known (Candelas and de la Ossa, 1990) and it looks like the total space of T^*S^3, with the volume of the S^3 shrinking to zero as $\epsilon^{3/2}$ when $\epsilon \to 0$.[11] Thus the smallest length scale on this noncompact CY is $L \sim \epsilon^{1/2}$. For $\epsilon \neq 0$, the solution of $\nabla f = 0$ is all $z_i = 0$, and the distance (in the Euclidean metric) from this point to the closest solution of $f = 0$ is also $\epsilon^{1/2}$.

In the limit $\epsilon \to 0$, the metric becomes singular, with Kähler potential

$$K \sim \left(z_1^2 + z_2^2 + z_3^2 + z_4^2\right)^{4/3} \tag{53}$$

near the singularity. This Kähler potential is a C^2 function for which one expects the Fourier coefficients to fall off as k^{-4}, which is consistent with the numerical results in Headrick and Nassar (2013). The Kähler form ω and the CY volume form $d\mu_\Omega$ (Equation (9)) should then be C^0, so one does not expect other numerical problems besides the large ratio of scales.

11. This can be seen by writing the real and imaginary parts of Equation (52) separately. For $\epsilon > 0$ real, the S^3 is the submanifold $\mathrm{Im} z_i = 0$.

To identify the region described by Equation (52) and ϵ in our equations such as Equation (34) and Equation (35), we use an idea from Blum et al. (1998). This is to first define the distance $d_Z(f, \Delta_Z)$ from a given f to Δ_Z, the subset of Δ for which $f(Z) = \partial f(Z) = 0$ for some $Z \in \mathbb{CP}^4$. We then minimize over Z,

$$d(f, \Delta) = \min_{Z \in M} d(f, \Delta_Z). \tag{54}$$

To define $d_Z(f, \Delta_Z)$, note that the subset of $\mathcal{M}$ for which $f(Z) = 0$ is a linear subspace, call it V_Z. Thus, we can use distance to Δ_Z in the Fubini-Study metric restricted to V_Z.[12] Let $||f||_H$ be the norm of f in this metric; a convenient way to express it is

$$||f||_H^2 = \mathcal{N} \int_{\mathbb{C}^5} e^{-|Z|^2} |f(Z)|^2, \tag{55}$$

while the constraints $\partial_i h = 0$ are best expressed in terms of a kernel

$$\mathcal{K}_n(Z, \bar{Z}) = H_{I\bar{J}} Z^I \bar{Z}^{\bar{J}} = \frac{1}{n!} (\sum_i Z_i \bar{Z}_{\bar{i}})^n. \tag{56}$$

Now, let $c_i \in V$ be the constraints $\partial_i Z^I$, with inner products

$$\begin{aligned} L_{i\bar{j}} &= c_i \cdot H \cdot c_{\bar{j}} && (57)\\ &= \frac{\partial}{\partial Z^i} \frac{\partial}{\partial \bar{Z}^{\bar{j}}} \mathcal{K}_n(Z, \bar{Z}) \Big|_{Z=Z_0} && (58)\\ &= \delta_{i\bar{j}} \mathcal{K}_{n-1}(Z, \bar{Z}) + \bar{Z}_i Z_{\bar{j}} \mathcal{K}_{n-2}(Z, \bar{Z}). && (59) \end{aligned}$$

Then the minimal distance from f to Δ_{Z_0} is the norm in the subspace given by the projection $P = (L^{-1})^{i\bar{j}} H \cdot c_i c_{\bar{j}}$.

$$\sin^2 \theta = \frac{\langle f, Pf \rangle_H}{||f||_H^2} = \frac{(L^{-1})^{i\bar{j}} \partial_i f \partial_{\bar{j}} \bar{f}|_{Z=Z_0}}{||f||_H^2}. \tag{60}$$

The denominator is independent of Z_0, and the matrix $\delta_{i\bar{j}} + (n-1)\bar{Z}_i Z_{\bar{j}}/|Z|^2$ is easy to invert. This will give combinations $|Z^i \partial_i f|^2 (n-1)/n = (n-1)n|f(Z_0)|^2 = 0$ and finally

$$\sin\theta \propto d \equiv \min_{Z_0 \in M} \frac{|\partial_i f(Z_0)|_H}{||f||_H |Z_0|^{n-1}}. \tag{61}$$

For our purposes it suffices to take the right hand side of this equation as our definition of distance, and to compute it in examples using numerical minimization.

We plot Eq. (61) for the Dwork quintics in Figure 6. Besides the conifold point at $\psi = -5$, there is a local minimum near $\psi = 5$, which fits with the feature seen in the plot of curvature versus ψ in Cui and Gray (2020). This is the point on the positive real axis closest to the conifold point, perhaps reached by following a path like $\psi = 5e^{i\theta}$. It would be nice to check this against the known exact metric for this example Candelas et al. (1991).

Heat map plots of Eq. (61) for the other defining functions appear in Figure 1(*a*)subfigure and Figure 1(*b*)subfigure.

12. This definition of distance depends on the choice of FS metric. In Blum et al. (1998) it was used to get expectations under a probability measure on hypersurfaces which also depended on this choice. But for our application, this is a deficiency. The symmetric choice we made gives reasonable results, but it would be interesting to remove this dependence, perhaps by using the balanced FS metric or best approximate Ricci flat metric adapted to M.

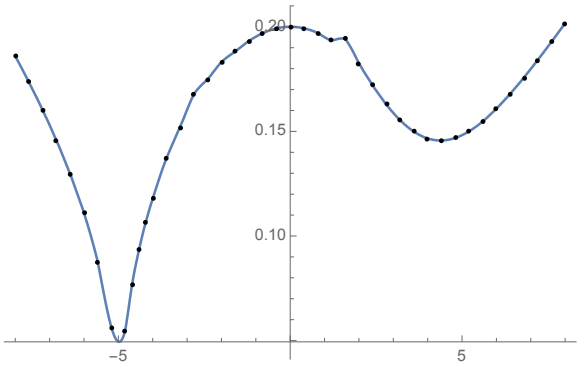

Figure 6: Distance to discriminant locus for the Dwork quintics, Eq. (3). X axis is ψ, Y axis is d in Eq. (61).